Domain walls of ferroelectric $BaTiO_3$ within the Ginzburg-Landau-Devonshire phenomenological model

P. Marton, I. Rychetsky, and J. Hlinka
Institute of Physics, Academy of Sciences of the Czech Republic, Na Slovance 2, 18221 Praha 8, Czech Republic
(Received 21 January 2010; revised manuscript received 30 March 2010; published 27 April 2010)

Mechanically compatible and electrically neutral domain walls in tetragonal, orthorhombic, and rhombohedral ferroelectric phases of $BaTiO_3$ are systematically investigated in the framework of the phenomenological Ginzburg-Landau-Devonshire model with parameters of J. Hlinka and P. Marton, Phys. Rev. B **74**, 104104 (2006). Polarization and strain profiles within domain walls are calculated numerically and within an approximation leading to the quasi-one-dimensional analytic solutions applied previously to the ferroelectric walls of the tetragonal phase [W. Cao and L. E. Cross, Phys. Rev. B **44**, 5 (1991)]. Domain-wall thicknesses and energy densities are estimated for all mechanically compatible and electrically neutral domain-wall species in the entire temperature range of ferroelectric phases. The model suggests that the lowest-energy walls in the orthorhombic phase of $BaTiO_3$ are the 90° and 60° walls. In the rhombohedral phase, the lowest-energy walls are the 71° and 109° walls. All these ferroelastic walls have thickness below 1 nm except for the 90° wall in the tetragonal phase and the 60° *S* wall in the orthorhombic phase, for which the larger thickness on the order of 5 nm was found. The antiparallel walls of the rhombohedral phase have largest energy and thus they are unlikely to occur. The calculation indicates that the lowest-energy structure of the 109° wall and few other domain walls in the orthorhombic and rhombohedral phases resemble Bloch walls known from magnetism.

DOI: 10.1103/PhysRevB.81.144125 PACS number(s): 77.80.Dj, 77.84.Cg

I. INTRODUCTION

Domain structure is an important ingredient in functionality of ferroelectric materials. Among others, it has impact on their nonlinear optical properties, dielectric permittivity, and polarization switching phenomena. Since domain boundaries in ferroelectric perovskite materials can simultaneously play the role of the ferroelectric and ferroelastic walls, such domain walls also strongly influence the electromechanical material properties: they facilitate switching of spontaneous polarization and spontaneous deformation, thus giving rise to a large extrinsic contribution to, e.g., piezoelectric constants, which makes ferroelectric materials extremely attractive for applications. The domain structure also provides additional degree of freedom for tuning of material properties. In general, further development of domain engineering strategies requires deeper understanding of the physics of ferroelectric domain wall itself.

The Ginzburg-Landau-Devonshire (GLD) theory provides a feasible tool for such a purpose. Landau-Devonshire model describes phase-transition properties of single-domain crystal using a limited number of parameters, which are determined experimentally (or recently also using *ab initio* methods). Introduction of Ginzburg gradient term to the free-energy functional enables addressing nonhomogeneous multidomain ferroelectric state. The GLD model was previously used for computation of domain-wall properties in ferroelectric materials (e.g., Refs. 1–5) and in phase-field computer modeling of domain formation and evolution.[6–9] The GLD model can be regarded as a bridge model covering length scales inaccessible by *ab initio* and micromechanical models.

$BaTiO_3$ (BTO) represents a typical ferroelectric material which undergoes a sequence of phase transitions from high-temperature paraelectric cubic $Rm\bar{3}m$ (O_h^1) to the ferroelectric tetragonal $P4mm$ (C_{4v}^1), orthorhombic $Amm2$ (C_{2v}^{14}), and rhombohedral $R3m$ (C_{3v}^5) phase. Energetically equivalent directions of spontaneous polarization vector, identifying possible ferroelectric domain states in a particular ferroelectric phase, are displayed in Fig. 1. Domain boundaries separating two domain states are characterized by the rotational angle needed to match spontaneous polarizations on both sides of the boundary. For example, the boundary separating domains with mutually perpendicular spontaneous polarization is commonly called 90° wall while the one between antiparallel spontaneous polarization regions is called 180° wall. Other angles are possible in orthorhombic and rhombohedral phases of $BaTiO_3$, where the spontaneous polarization is oriented along the cubic face diagonals and body diagonals, respectively.

Estimation of the 90° domain-wall thickness in the tetragonal phase of $BaTiO_3$ agrees reasonably well with experimental observations, as can be seen from the detailed summary of the recent experimental data in Table IV of Ref. 4. A relevant first-principles results on BTO and related materials are provided in the same work as well. The aim of this paper is to extend the previous work and to calculate basic characteristics of all electrically neutral and mechanically compat-

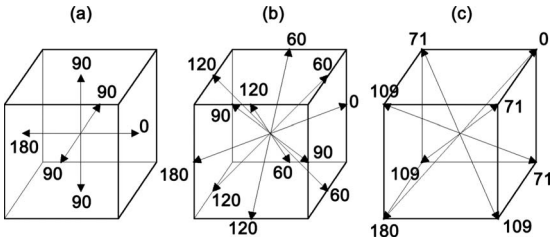

FIG. 1. Directions of spontaneous polarization in (a) the tetragonal, (b) orthorhombic, and (c) rhombohedral phase. Angles between polarization direction "0" and its symmetry equivalent ones are indicated.

ible domain walls in all ferroelectric phases of $BaTiO_3$. For a better comparison of domain-wall properties such as their thickness or energy density, we employ an Ising-type approximation leading to previously proposed analytically solvable one-dimensional solutions.[1] The paper is organized as follows. In Sec. II, we give an overview of the different kinds of mechanically compatible domain walls in the three ferroelectric phases. It follows from general theory about macroscopic mechanical compatibility of adjacent domain states.[10,11] The GLD parameters used for calculation of the domain-wall properties in $BaTiO_3$ are the same as in our preceding work[4] but for the sake of convenience, the definition and the GLD model and its parameters are resumed in Sec. III. Section IV is devoted to description of the computational scheme and approximations applied here to solve analytically the Euler-Lagrange equations. The main result of our study—systematic numerical evaluation of thicknesses, energies, polarization profiles, and other properties for different domain walls, is presented in Sec. V. Sections VI and VII are devoted to the discussion of validity of used approximations and final conclusion, respectively.

II. MECHANICALLY COMPATIBLE DOMAIN WALLS IN BARIUM TITANATE

The energy degeneracy of different directions of spontaneous polarization leads to the appearance of ferroelectric domain structure. Individual domains are separated by domain walls, where the polarization changes from one state to another. As only planar domain walls are considered here, we denote the vector of spontaneous polarization and tensor of spontaneous deformation on one side of the domain wall $\mathbf{P}(-\infty)$ and $\mathbf{e}(-\infty)$, and $\mathbf{P}(\infty)$ and $\mathbf{e}(\infty)$ on the other side. The argument ∞ stresses that the spontaneous values are taken at a sufficient distance from the domain wall. An orientation of a mechanically compatible domain wall with the normal (x_1,x_2,x_3) can be determined from the equation for mechanically compatible interfaces separating two domains with the strain tensors $e_{ij}(-\infty)$ and $e_{ij}(\infty)$,

$$\sum_{m,n=1}^{3} [e_{mn}(\infty) - e_{mn}(-\infty)]x_m x_n = 0. \quad (1)$$

Systematic analysis of this equation using symmetry arguments has been done, e.g., in Refs. 10–12. In general, the number N of mechanically compatible domain walls separating two particular domain states can have only one of the three values: $N=0$, $N=2$, or $N=\infty$. In case of $N=2$, there exist two mutually perpendicular domain walls. Each of them is either a crystallographic (W_f-type) wall or noncrystallographic (S-type) wall. Orientation of the W_f wall is fixed by symmetry of the crystal while orientation of the S wall is determined by components of the strain tensor in adjacent domains (and its orientation can be therefore dependent on temperature). For $N=\infty$, there exists infinite number of wall orientations, some of them may be preferred energetically.

Further, the electrically neutral domain walls will be considered.[10] It implies that the difference $\mathbf{P}(\infty)-\mathbf{P}(-\infty)$ between the spontaneous polarizations in the adjacent domains is perpendicular to the unit vector $\mathbf{s}$, normal to the domain wall,

$$[\mathbf{P}(\infty) - \mathbf{P}(-\infty)] \cdot \mathbf{s} = 0. \quad (2)$$

We also define a unit vector $\mathbf{r} \| [\mathbf{P}(\infty)-\mathbf{P}(-\infty)]$, which identifies the component of the spontaneous polarization which reverses when crossing the wall. Then the charge neutrality condition (2) can be expressed as $\mathbf{r}\cdot\mathbf{s}=0$. Finally, let us introduce a third base vector $\mathbf{t}=\mathbf{r}\times\mathbf{s}$, which complements the symmetry-adapted orthonormal coordinate system (r, s, t).

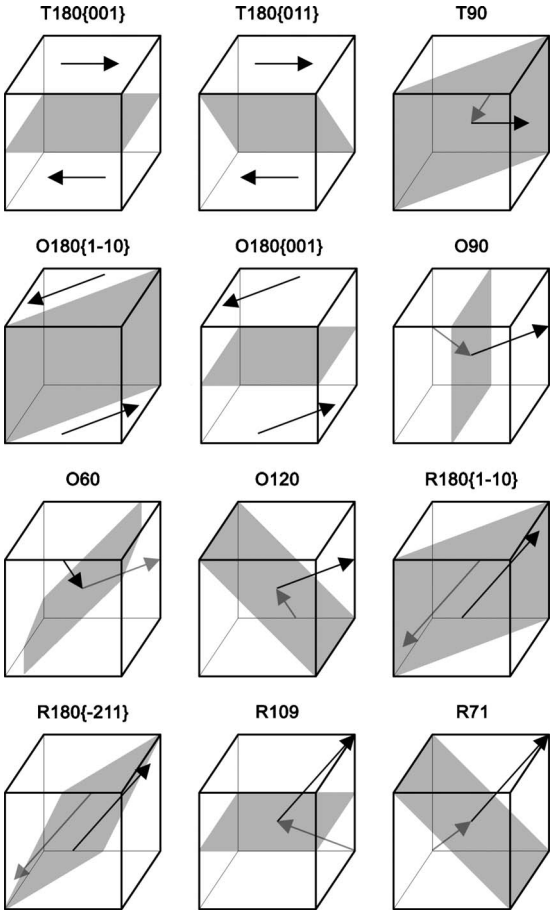

FIG. 2. Set of mechanically compatible and electrically neutral domain walls in the three ferroelectric phases of $BaTiO_3$. In the case of 180° domain walls, where the orientation is not determined by symmetry, walls with the most important crystallographic orientations are displayed.

$BaTiO_3$ symmetry allows a variety of domain walls.[12] Ferroelectric walls of $BaTiO_3$ can be divided in two groups—the nonferroelastic walls separating domains with antiparallel polarization $[e_{mn}(\infty)-e_{mn}(-\infty)=0, N=\infty]$ and the ferroelastic walls with other than 180° between polarization in the adjacent domain states ($N=2$). The $\mathbf{r}\cdot\mathbf{s}=0$ condition implies that the neutral nonferroelastic walls are parallel to the spontaneous polarization, and the neutral ferroelastic walls realize a "head-to-tail" junction. The set of plausible neutral and mechanically compatible domain wall types are schematically shown in Fig. 2. Domain walls are labeled by a symbol composed of the letter specifying the ferroelectric

TABLE I. Cartesian components of switching vectors **r**, domain-wall normals **s**, and boundary conditions for polarization and strain in adjacent domain states for the inspected domain walls. Vector $\mathbf{s}_{O60}$ is defined in Eq. (3), P_0 stands for magnitude of spontaneous polarization. As usual, spontaneous quantities are those minimizing GLD functional. Numerical values used in this work are given in Sec. V.

Wall	**r**	**s**	$\mathbf{P}(-\infty)/P_0$	$\mathbf{P}(\infty)/P_0$	$\mathbf{e}(-\infty)$	$\mathbf{e}(\infty)$
T180{001}	(1,0,0)	(0,0,1)	(1,0,0)	(−1,0,0)	$(e_\parallel,e_\perp,e_\perp,0,0,0)$	$(e_\parallel,e_\perp,e_\perp,0,0,0)$
T180{011}	(1,0,0)	$(0,\frac{1}{\sqrt{2}},\frac{1}{\sqrt{2}})$	(1,0,0)	(−1,0,0)	$(e_\parallel,e_\perp,e_\perp,0,0,0)$	$(e_\parallel,e_\perp,e_\perp,0,0,0)$
T90	$(\frac{1}{\sqrt{2}},\frac{1}{\sqrt{2}},0)$	$(\frac{1}{\sqrt{2}},\frac{-1}{\sqrt{2}},0)$	(1,0,0)	(0,−1,0)	$(e_\parallel,e_\perp,e_\perp,0,0,0)$	$(e_\perp,e_\parallel,e_\perp,0,0,0)$
O180{1$\bar{1}$0}	$(\frac{1}{\sqrt{2}},\frac{1}{\sqrt{2}},0)$	$(\frac{1}{\sqrt{2}},\frac{-1}{\sqrt{2}},0)$	$(\frac{1}{\sqrt{2}},\frac{1}{\sqrt{2}},0)$	$(\frac{-1}{\sqrt{2}},\frac{-1}{\sqrt{2}},0)$	$(e_a,e_a,e_c,0,0,2e_b)$	$(e_a,e_a,e_c,0,0,2e_b)$
O180{001}	$(\frac{1}{\sqrt{2}},\frac{1}{\sqrt{2}},0)$	(0,0,1)	$(\frac{1}{\sqrt{2}},\frac{1}{\sqrt{2}},0)$	$(\frac{-1}{\sqrt{2}},\frac{-1}{\sqrt{2}},0)$	$(e_a,e_a,e_c,0,0,2e_b)$	$(e_a,e_a,e_c,0,0,2e_b)$
O90	(0,1,0)	(1,0,0)	$(\frac{1}{\sqrt{2}},\frac{1}{\sqrt{2}},0)$	$(\frac{1}{\sqrt{2}},\frac{-1}{\sqrt{2}},0)$	$(e_a,e_a,e_c,0,0,2e_b)$	$(e_a,e_a,e_c,0,0,-2e_b)$
O60	$(\frac{1}{\sqrt{2}},0,\frac{1}{\sqrt{2}})$	$\mathbf{s}_{O60}$	$(\frac{1}{\sqrt{2}},\frac{1}{\sqrt{2}},0)$	$(0,\frac{1}{\sqrt{2}},\frac{-1}{\sqrt{2}})$	$(e_a,e_a,e_c,0,0,2e_b)$	$(e_c,e_a,e_a,-2e_b,0,0)$
O120	$(\frac{1}{\sqrt{6}},\frac{2}{\sqrt{6}},\frac{-1}{\sqrt{6}})$	$(\frac{1}{\sqrt{2}},0,\frac{1}{\sqrt{2}})$	$(\frac{1}{\sqrt{2}},\frac{1}{\sqrt{2}},0)$	$(0,\frac{-1}{\sqrt{2}},\frac{1}{\sqrt{2}})$	$(e_a,e_a,e_c,0,0,2e_b)$	$(e_c,e_a,e_a,-2e_b,0,0)$
R180{1$\bar{1}$0}	$(\frac{1}{\sqrt{3}},\frac{1}{\sqrt{3}},\frac{1}{\sqrt{3}})$	$(\frac{1}{\sqrt{2}},\frac{-1}{\sqrt{2}},0)$	$(\frac{1}{\sqrt{3}},\frac{1}{\sqrt{3}},\frac{1}{\sqrt{3}})$	$(\frac{-1}{\sqrt{3}},\frac{-1}{\sqrt{3}},\frac{-1}{\sqrt{3}})$	$(e_a,e_a,e_a,2e_b,2e_b,2e_b)$	$(e_a,e_a,e_a,2e_b,2e_b,2e_b)$
R180{$\bar{2}$11}	$(\frac{1}{\sqrt{3}},\frac{1}{\sqrt{3}},\frac{1}{\sqrt{3}})$	$(\frac{-2}{\sqrt{6}},\frac{1}{\sqrt{6}},\frac{1}{\sqrt{6}})$	$(\frac{1}{\sqrt{3}},\frac{1}{\sqrt{3}},\frac{1}{\sqrt{3}})$	$(\frac{-1}{\sqrt{3}},\frac{-1}{\sqrt{3}},\frac{-1}{\sqrt{3}})$	$(e_a,e_a,e_a,2e_b,2e_b,2e_b)$	$(e_a,e_a,e_a,2e_b,2e_b,2e_b)$
R109	$(\frac{1}{\sqrt{2}},\frac{1}{\sqrt{2}},0)$	(0,0,1)	$(\frac{1}{\sqrt{3}},\frac{1}{\sqrt{3}},\frac{1}{\sqrt{3}})$	$(\frac{-1}{\sqrt{3}},\frac{-1}{\sqrt{3}},\frac{1}{\sqrt{3}})$	$(e_a,e_a,e_a,2e_b,2e_b,2e_b)$	$(e_a,e_a,e_a,-2e_b,-2e_b,2e_b)$
R71	(0,1,0)	$(\frac{1}{\sqrt{2}},0,\frac{1}{\sqrt{2}})$	$(\frac{1}{\sqrt{3}},\frac{1}{\sqrt{3}},\frac{1}{\sqrt{3}})$	$(\frac{1}{\sqrt{3}},\frac{-1}{\sqrt{3}},\frac{1}{\sqrt{3}})$	$(e_a,e_a,e_a,2e_b,2e_b,2e_b)$	$(e_a,e_a,e_a,-2e_b,2e_b,-2e_b)$

phase (T, O, or R staying for the tetragonal, orthorhombic or rhombohedral, respectively), number indicating the polarization rotation angle (180°, 120°, 109°, 90°, 71°, or 60°) and, if needed, the orientation of the domain wall normal with respect to the parent pseudocubic reference structure.

Our choice of the base vectors **r**, **s** and of the spontaneous polarization and strain components in the adjacent domain pairs for each domain-wall type shown in Fig. 2 are summarized in Table I. Base vectors coincide with special crystallographical directions, except for the O60 wall where the **s** and **t** vectors depend on the orthorhombic spontaneous strain (see Table I) as follows:[5]

$$\mathbf{r}_{O60}=\left(\frac{1}{\sqrt{2}},0,\frac{1}{\sqrt{2}}\right),$$

$$\mathbf{s}_{O60}=\left(\frac{e_a-e_c}{D_1},\frac{2e_b}{D_1},\frac{e_c-e_a}{D_1}\right),$$

$$\mathbf{t}_{O60}=\left(\frac{-e_b}{D_2},\frac{e_a-e_c}{D_2},\frac{e_b}{D_2}\right) \tag{3}$$

with $D_1=\sqrt{2}D_2$, $D_2=\sqrt{(e_a-e_c)^2+2e_b^2}$ and with e_a, e_b, and e_c defined in Table I.

Although only the neutral walls are discussed in the following, the Fig. 2 is actually helpful in enumeration of all possible mechanically compatible domain wall species in $BaTiO_3$. In principle, mechanical compatibility allows 180° W_∞-type domain walls with an arbitrary orientation of the domain wall in all three ferroelectric phases (T180, O180, and R180). Obviously, they are electrically neutral only if the domain wall normal is parallel with the spontaneous polarization. Ferroelastic walls exists in mutually perpendicular pairs. In the tetragonal phase, there exist 90° W_f-type domain walls (T90), either charged (head-to-head or tail-to-tail) or neutral (head-to-tail). The orthorhombic phase is more complex. In the case of 60° angle between polarization directions, the $N=2$ pair is formed by a charged W_f-type wall and neutral S-type wall. The case of 120° angle is similar but W_f wall is neutral and S wall is charged. In addition, there are again charged or neutral 90° W_f walls (O90). The rhombohedral phase has pairs of charged and neutral W_f-type domain walls with the angle between polarizations either 109° or 71° (R109 or R71, respectively). Since only neutral walls are discussed here, the S type domain wall will be referred to as O60 and W_f wall as O120.

III. GLD MODEL FOR BARIUM TITANATE

Calculations presented in this paper are based on the GLD model with anisotropic gradient terms, reviewed in Ref. 4. The free energy F is expressed in terms of polarization and strain field taken for primary and secondary order parameter, respectively,

$$F[\{P_i,P_{i,j},u_{ij}\}]=\int f d\mathbf{r}, \tag{4}$$

where the free-energy density f consists of Landau, gradient, elastic, and electrostriction part,

$$f=f_L^{(e)}\{P_i\}+f_C\{P_i,e_{ij}\}+f_q\{P_i,e_{ij}\}+f_G\{P_{i,j}\}. \tag{5}$$

The Landau potential considered here is expanded up to the sixth order[13] in components of polarization for the cubic symmetry (O_h^1),

$$\begin{aligned}f_L^{(e)}=&\alpha_1(P_1^2+P_2^2+P_3^2)+\alpha_{11}^{(e)}(P_1^4+P_2^4+P_3^4)\\&+\alpha_{12}^{(e)}(P_1^2P_2^2+P_2^2P_3^2+P_1^2P_3^2)+\alpha_{111}(P_1^6+P_2^6+P_3^6)\\&+\alpha_{112}[P_1^4(P_2^2+P_3^2)+P_2^4(P_1^2+P_3^2)+P_3^4(P_1^2+P_2^2)]\\&+\alpha_{123}P_1^2P_2^2P_3^2\end{aligned} \tag{6}$$

with the three temperature-dependent coefficients α_1, α_{11} and α_{111}, as in Ref. 14. This expansion produces the six equivalent domain states in the tetragonal phase, twelve in

the orthorhombic, and eight in the rhombohedral phase (see Fig. 1).

Dependence of the free energy on the strain is encountered by including elastic and linear-quadratic electrostriction functionals F_C and F_q, respectively. Their corresponding free energy densities are

$$f_C = \frac{1}{2} C_{ijkl} e_{ij} e_{kl} \tag{7}$$

and

$$f_q = - q_{ijkl} e_{ij} P_k P_l, \tag{8}$$

where $e_{ij} = \frac{1}{2}(\partial u_i / \partial x_j + \partial u_j / \partial x_i)$. C_{ijkl} and q_{ijkl} are components of elastic and electrostriction tensor. In following, we use Voigt notation in which $C_{11}=C_{1111}$, $C_{12}=C_{1122}$, $C_{44}=C_{1212}$, $q_{11}=q_{1111}$, and $q_{12}=q_{1122}$ but $q_{44}=2q_{1122}$. Abbreviated form of e_{ij} is as usual.

The elastic and electrostriction terms result in renormalization of the bar expansion coefficients $\alpha_{11}^{(e)}$ and $\alpha_{12}^{(e)}$ when minimizing the free energy with respect to strains (in the homogeneous sample). The bar $\alpha_{11}^{(e)}$, $\alpha_{12}^{(e)}$ and the relaxed α_{11}, α_{12} coefficients are related as[4]

$$\alpha_{11}^{(e)} = \alpha_{11} + \frac{1}{6}\left[\frac{\hat{q}_{11}^2}{\hat{C}_{11}} + 2\frac{\hat{q}_{22}^2}{\hat{C}_{22}}\right],$$

$$\alpha_{12}^{(e)} = \alpha_{12} + \frac{1}{6}\left[2\frac{\hat{q}_{11}^2}{\hat{C}_{11}} - 2\frac{\hat{q}_{22}^2}{\hat{C}_{22}} + 3\frac{q_{44}^2}{C_{44}}\right] \tag{9}$$

with

$$\hat{C}_{11} = C_{11} + 2C_{12},$$

$$\hat{C}_{22} = C_{11} - C_{12},$$

$$\hat{q}_{11} = q_{11} + 2q_{12},$$

$$\hat{q}_{22} = q_{11} - q_{12}. \tag{10}$$

The Ginzburg gradient term f_G is considered in the form

$$f_G = \frac{1}{2} G_{11}(P_{1,1}^2 + P_{2,2}^2 + P_{3,3}^2) + G_{12}(P_{1,1}P_{2,2} + P_{2,2}P_{3,3} + P_{1,1}P_{3,3}) + \frac{1}{2} G_{44}[(P_{1,2} + P_{2,1})^2 + (P_{2,3} + P_{3,2})^2 + (P_{3,1} + P_{1,3})^2]. \tag{11}$$

It was pointed out[4] that the tensor of gradient constants of $BaTiO_3$ is highly anisotropic with fundamental consequences on predicted domain-wall properties. Up to now, the isotropic gradient tensor $G_{i,j}$ was mostly employed in the computations.

The material-specific coefficients in the model are assumed being constant, except for the three Landau potential coefficients,

$$\alpha_1 = 3.34 \times 10^5 (T - 381),$$

$$\alpha_{11} = 4.69 \times 10^6 (T - 393) - 2.02 \times 10^8,$$

$$\alpha_{111} = -5.52 \times 10^7 (T - 393) + 2.76 \times 10^9, \tag{12}$$

where T is absolute temperature.[14] The phase transitions occur in this model at the temperatures 392.3 K (C→T), 282.5 K (T→O), and 201.8 K (O→R). All phase transitions are of the first order, the local minima corresponding to the tetragonal, orthorhombic, and rhombohedral phase exist for this Landau potential between 237 K and 393 K, between 104 K and 303 K, and below 256 K, respectively. Full set of temperature-independent parameters of the GLD model reads[4,15] $\alpha_{12}=3.230\times10^8$ J m^5 C^{-4}, $\alpha_{112}=4.470\times10^9$ J m^9 C^{-6}, $\alpha_{123}=4.910\times10^9$ J m^9 C^{-6}, $G_{11}=51\times10^{-11}$ J m^3 C^{-2}, $G_{12}=-2\times10^{-11}$ J m^3 C^{-2}, $G_{44}=2\times10^{-11}$ J m^3 C^{-2}, $q_{11}=14.20\times10^9$ J m C^{-2}, $q_{12}=-0.74\times10^9$ J m C^{-2}, $q_{44}=1.57\times10^9$ J m C^{-2}, $C_{11}=27.50\times10^{10}$ J m^{-3}, $C_{12}=17.90\times10^{10}$ J m^{-3}, and $C_{44}=5.43\times10^{10}$ J m^{-3}.

IV. STRAIGHT POLARIZATION PATH APPROXIMATION

Let us consider a single mechanically compatible and electrically neutral domain wall in a perfect infinite stress-free crystal. Within the continuum GLD theory, such domain wall is associated with a planar kink solution of the Euler-Lagrange equations of the GLD functional for polarization vector and the strain tensor.[1,2,4,17] Domain-wall type is specified by selection of the wall normal **s** and by the two domain states at $s=-\infty$ and $+\infty$. This ideal geometry implies that the polarization and strain vary only along normal to the wall **s** and domain wall can be thus considered as a trajectory in order-parameter space.

Even if the domain wall is neutral, in its central part the local electric charges can occur due to the position-dependent polarization. The additional assumption $\nabla \cdot \mathrm{P}=0$ ensures the absence of charges in the whole domain wall. Then the local electric field is zero and the electrostatic contribution vanishes. Such strictly charge-free solutions[17] were found to be an excellent approximation for ideal dielectric materials.[4] The condition $\nabla \cdot \mathrm{P}=0$ implies that the polarization vector variation is restricted to a plane perpendicular to **s** [the trajectory is constrained to $P_s=P_s(\pm\infty)$ plane].

In fact, the polarization trajectories representing the T180 and T90 walls calculated under $\nabla \cdot \mathrm{P}=0$ constraint were found to be the straight lines connecting the boundary values.[1,2,4,17] This greatly simplifies the algebra and the solution of the variational problem can be found analytically. Therefore, we decided to impose the condition of a direct, straight polarization trajectory for the variational problem of all domain wall species of $BaTiO_3$. This condition, further referred as straight polarization path (SPP) approximation, implies that both P_s and P_t polarization components are constant across the wall. We shall come back to the meaning and possible drawbacks of this approximation in Sec. VI.

Polarization and strain in the mechanically compatible and electrically neutral SPP walls can be cast in the form

$\mathbf{P}=[P_r(s),P_s(\pm\infty),P_t(\pm\infty)]$ and $e=[e_{rr}(\pm\infty),e_{ss}(s),e_{tt}(\pm\infty),2e_{st}(s),2e_{rt}(\pm\infty),2e_{rs}(s)]$, respectively. The s-dependent strain components are calculated from the mechanical equilibrium condition,

$$\sum_{j=1}^{3}\frac{\partial\sigma_{ij}}{\partial x_j}=\sum_{j=1}^{3}\frac{\partial}{\partial x_j}\left(\frac{\partial f}{\partial e_{ij}}\right)=0. \tag{13}$$

Boundary conditions for stress and the fact that all quantities vary only along direction s imply

$$\frac{\partial f_{\mathrm{Cq}}}{\partial e_{ij}}+C=0 \tag{14}$$

for $ij\in\{\mathrm{ss},\mathrm{st},\mathrm{rs}\}$ with the integration constant C to be determined from boundary conditions.

The Euler-Lagrange equation for polarization reduces to

$$\frac{\partial}{\partial s}\frac{\partial f}{\partial P_{r,s}}-\frac{\partial f}{\partial P_r}=0, \tag{15}$$

where the strain components from Eq. (14) were substituted into f. Thus, the elastic field was eliminated. It turns out that the resulting Euler-Lagrange equation for P_r is possible to rewrite in the form

$$g\frac{d^2p(s)}{ds^2}=2a_1p(s)+4a_{11}p^3(s)+6a_{111}p^5(s), \tag{16}$$

where $p(s)$ stands for $P_r(s)$, and where the coefficients g, a_1, a_{11} and a_{111}, different for each domain type, depend only on the material tensors. The boundary values are $-P_r(\infty)=P_r(-\infty)=p_\infty$.

Solution of the Euler-Lagrange Eq. (16) is well known.[1,17–20] We shall follow the procedure of Ref. 21. Integrating Eq. (16), one can obtain the equation,

$$\frac{g}{2}\left(\frac{\partial p}{\partial s}\right)^2=f_{\mathrm{EL}}(p), \tag{17}$$

where (see Ref. 4)

$$f_{\mathrm{EL}}(p)=a_1p(s)^2+a_{11}p(s)^4+a_{111}p(s)^6. \tag{18}$$

The function $f_{\mathrm{EL}}(p)$ is a double-well "Euler-Lagrange" potential with two minima $\pm p_\infty$, where

$$p_\infty^2=\frac{-a_{11}+\sqrt{a_{11}^2-3a_{111}a_1}}{3a_{111}}. \tag{19}$$

The differential Eq. (16) has the analytical solution

$$p(s)=p_\infty\frac{\sinh(s/\xi')}{\sqrt{A+\sinh^2(s/\xi')}}, \tag{20}$$

where

$$A=\frac{3a_{111}p_\infty^2+a_{11}}{2a_{111}p_\infty^2+a_{11}} \tag{21}$$

and

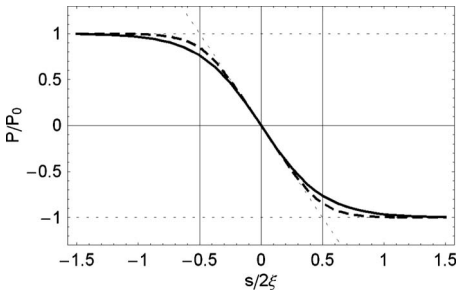

FIG. 3. Profile of the "reversed" polarization component P_r [Eq. (20)] for a domain wall with the shape factor $A=1$ (solid) and $A=3$ (dashed). Both profiles have the same derivative for $s/2\xi=0$ (dotted) and therefore also the same thickness (indicated by vertical lines) according to the definition in Eq. (23).

$$\xi'=\frac{\xi}{\sqrt{A}}. \tag{22}$$

Quantity A determines deviation of the profile [Eq. (20)] from the tanh profile, which occurs for the fourth-order potential (i.e., $a_{111}=0$, $A=1$).

The domain wall thickness (Fig. 3) is defined as

$$2\xi=p_\infty\sqrt{\frac{2g}{U}} \tag{23}$$

with U being the energy barrier between the domain states,

$$U=f_{\mathrm{EL}}(0)-f_{\mathrm{EL}}(p_\infty)=2a_{111}p_\infty^6+a_{11}p_\infty^4. \tag{24}$$

The surface energy density of the domain wall is

$$\Sigma=\int_{-\infty}^{\infty}[f_{\mathrm{EL}}(s)-f_{\mathrm{EL}}(p_\infty)]ds=\frac{4}{3}p_\infty\sqrt{2gU}[A^{5/2}I(A)], \tag{25}$$

where

$$I(A)=\frac{3}{4}\int_{-\infty}^{\infty}\frac{\cosh^2(t)dt}{[A+\cosh^2(t)-1]^3}. \tag{26}$$

The domain-wall characteristics depend on the coefficients g, a_1, a_{11}, a_{111} through Eqs. (19), (20), (23), and (25). The explicit expressions for these coefficients are summarized for various domain walls in Table II. The expressions are simplified using the notation inspired by Ref. 1. For all phases we are using

$$a_1^r=\alpha_1-\left[\frac{1}{3}\frac{\hat{q}_{11}^2}{\hat{C}_{11}}+\frac{1}{6}\frac{\hat{q}_{22}^2}{\hat{C}_{22}}-\frac{(q_{11}+q_{12})q'_{12}}{2C'_{11}}\right]P_0^2,$$

$$a_{11}^r=\frac{\alpha_{11}^{(e)}}{2}+\frac{\alpha_{12}^{(e)}}{4}-\frac{q'^2_{12}}{2C'_{11}},$$

$$a_{12}^{rs}=3\alpha_{11}^{(e)}-\frac{\alpha_{12}^{(e)}}{2}-\frac{q'_{11}q'_{12}}{C'_{11}}-\frac{\hat{q}_{22}^2}{2\hat{C}_{22}},$$

TABLE II. Parameters characterizing various mechanically compatible and neutral domain-wall species of $BaTiO_3$-like ferroelectrics within the SPP treatment described in the Sec. IV. Results for O60, O120, and R180{$\bar{2}$11} walls as well as a few other parameters are omitted because the corresponding analytical expressions through the GLD model parameters and spontaneous values of polarization and strain are too complicated.

Domain wall	p_∞	g	a_1	a_{11}	a_{111}
			Tetragonal phase		
T180{001}	P_0	G_{44}	$\alpha_1-e_\parallel q_{11}-e_\perp q_{12}+\frac{C_{12}}{C_{11}}(e_\parallel+e_\perp)q_{12}$	$\alpha_{11}^{(e)}-\frac{1}{2}\frac{q_{12}^2}{C_{11}}$	α_{111}
T180{011}	P_0	G_{44}	$\alpha_1-e_\parallel q_{11}+\frac{C_{12}}{C'_{11}}e_\parallel q_{12}-2\frac{C_{44}}{C'_{11}}e_\perp q_{12}$	$\alpha_{11}^{(e)}-\frac{1}{2}\frac{q_{12}^2}{C'_{11}}$	α_{111}
T90	$\frac{P_0}{\sqrt{2}}$	$\frac{G_{11}-G_{12}}{2}$	$\alpha_1^{\mathrm{r}}+\alpha_{12}^{\mathrm{rs}}\frac{P_0^2}{2}+\alpha'_{112}\frac{P_0^4}{4}$	$\alpha_{11}^{\mathrm{r}}+\alpha'_{112}\frac{P_0^2}{2}$	α'_{111}
			Orthorhombic phase		
O180{1$\bar{1}$0}	P_0	$\frac{G_{11}-G_{12}}{2}$	$\alpha_1-e_b(q'_{11}-q'_{12})-e_c q_{12}-e_a(q'_{11}+q'_{12})+\frac{q_{12}'^2}{C'_{11}}P_0^2$	$\frac{\alpha_{11}^{(e)}}{2}+\frac{\alpha_{12}^{(e)}}{4}-\frac{q_{12}'^2}{2C'_{11}}$	$\frac{1}{4}(\alpha_{111}+\alpha_{112})$
O180{001}	P_0	G_{44}	$\alpha_1-e_a(q_{11}+q_{12})-e_b q_{44}+2e_a q_{12}\frac{C_{12}}{C_{11}}$	$\frac{\alpha_{11}^{(e)}}{2}+\frac{\alpha_{12}^{(e)}}{4}-\frac{q_{12}^2}{2C_{11}}$	$\frac{1}{4}(\alpha_{111}+\alpha_{112})$
O90	$\frac{P_0}{\sqrt{2}}$	G_{44}	$\alpha_1^{\mathrm{r}}+\alpha_{12}^{(\mathrm{e})}\frac{P_0^2}{2}+\alpha_{112}\frac{P_0^4}{4}$	$\alpha_{11}^{(e)}+\frac{1}{2}[\alpha_{112}P_0^2-\frac{q_{12}^2}{C_{11}}]$	α_{111}
O120	$\frac{\sqrt{3}P_0}{2}$	$\frac{G_{11}-G_{12}+4G_{44}}{6}$	***	***	$\frac{2\alpha_{111}+21\alpha_{112}+2\alpha_{123}}{108}$
			Rhombohedral phase		
R180{1$\bar{1}$0}	P_0	$\frac{G_{11}-G_{12}+G_{44}}{3}$	$\alpha_1+\frac{1}{6C'_{33}}[C_{12}(e_a(q_{11}+2q_{12}-4q_{44})-6e_b q_{44})-C_{11}(6e_b q_{44}+3e_a q'_{11})-2C_{44}(3e_a(q_{11}+2q_{12})+6e_b q'_{11})]$	$\frac{\alpha_{11}^{(e)}+\alpha_{12}^{(e)}}{3}-\frac{q_{13}'^2}{2C'_{33}}$	$\frac{3\alpha_{111}+6\alpha_{112}+\alpha_{123}}{27}$
R180{$\bar{2}$11}	P_0	$\frac{G_{11}-G_{12}+G_{44}}{3}$	***	***	$\frac{3\alpha_{111}+6\alpha_{112}+\alpha_{123}}{27}$
R109	$\frac{P_0}{\sqrt{3}}$	G_{44}	$\alpha_1+\frac{\alpha_{12}^{(e)}P_0^2}{3}+\frac{\alpha_{112}P_0^4}{9}+\frac{2q_{12}^2P_0^2}{3C_{11}}-\frac{q_{44}^2P_0^2}{6C_{44}}-e_a(q_{11}+2q_{12})-e_b q_{44}$	$\frac{\alpha_{11}^{(e)}}{2}+\frac{\alpha_{12}^{(e)}}{4}-\frac{q_{12}^2}{2C_{11}}+\frac{1}{12}(2\alpha_{112}+\alpha_{123})P_0^2$	$\frac{\alpha_{111}+\alpha_{112}}{4}$
R71	$\frac{P_0}{\sqrt{3}}$	G_{44}	$\alpha_1+\frac{2\alpha_{12}^{(e)}P_0^2}{3}+\frac{2\alpha_{112}P_0^4}{9}+\frac{\alpha_{123}P_0^4}{9}-e_a(q_{11}+2q_{12})+\frac{q_{12}^2P_0^2}{3C'_{33}}-\frac{q_{44}^2P_0^2}{3C_{44}}$	$\alpha_{11}^{(e)}+\frac{2\alpha_{112}P_0^2}{3}-\frac{q_{12}^2}{2C'_{33}}$	α_{111}

$$a'_{111}=\frac{1}{4}(\alpha_{111}+\alpha_{112}),$$

$$a'_{112}=\frac{1}{4}(15\alpha_{111}-\alpha_{112}),$$

for tetragonal and orthorhombic phases, we are abbreviating

$$C'_{11}=\frac{C_{11}+C_{12}+2C_{44}}{2},$$

$$C'_{12}=\frac{C_{11}+C_{12}-2C_{44}}{2},$$

$$C'_{66}=\frac{C_{11}-C_{12}}{2},$$

$$q'_{11}=\frac{q_{11}+q_{12}+q_{44}}{2},$$

$$q'_{12}=\frac{q_{11}+q_{12}-q_{44}}{2},$$

$$q'_{66}=q_{11}-q_{12}$$

and for the rhombohedral phase

$$C'_{33}=\frac{C_{11}+C_{12}+2C_{44}}{2},$$

$$q'_{11}=\frac{q_{11}+2q_{12}+2q_{44}}{3},$$

$$q'_{13}=\frac{q_{11}+2q_{12}-q_{44}}{3}. \quad (27)$$

The expressions for the coefficients of the T180 and T90 domain walls are equivalent to the previously published expressions.[1,4] Derivations for O60, O120, and R180{$\bar{2}$11} walls lead to complicated formulas, and therefore only numerical results for g, a_1, a_{11}, and a_{111} coefficients are presented here.

V. QUANTITATIVE RESULTS

Advantage of the GLD approach is that domain-wall properties can be obtained at any temperature. In the Table III, we give numerical results for domain-wall parameters at one particular temperature for each of the ferroelectric phases: at 298 K, 208 K, and 118 K for the tetragonal, orthorhombic, and rhombohedral phase, respectively. Corresponding numerical values of the spontaneous quantities appearing in Table I are $P_0=0.265$ C m^{-2}, $e_\parallel=Q_{11}P_0^2=7.77\times10^{-3}$, and $e_\perp=Q_{12}P_0^2=-3.18\times10^{-3}$ (the tetragonal phase, 298 K); P_0

TABLE III. Predicted values of thickness and planar energy density of domain-wall species illustrated in Fig. 2 together with the determining parameters appearing in the SPP treatment. Results are evaluated from the $BaTiO_3$-specific GLD model at three selected temperatures corresponding to the tetragonal, orthorhombic, and rhombohedral phase, respectively. Domain walls for which relaxing of the P_t component results in a lower-energy CPP solution denoted by†. Numerical values are in SI units (2ξ in nm; Σ in mJ/m^2; U in MJ/m^3; p_∞ in C/m^2; g in 10^{-11} kg m^5 s^{-2} C^{-2}; a_1 in 10^7 kg m^3 s^{-2} C^{-2}; a_{11} in 10^8 kg m^7 s^{-2} C^{-4} ; a_{111} in 10^9 kg m^{11} s^{-2} C^{-6}).

Domain wall	2ξ	Σ	U	A	p_∞	g	a_1	a_{11}	a_{111}
				Tetragonal phase (298 K)					
T180{001}	0.63	5.9	6.41	1.43	0.265	2.0	−14.26	1.69	8.00
T180{011}	0.63	5.9	6.41	1.43	0.265	2.0	−14.26	1.69	8.00
T90	3.59	7.0	1.45	1.09	0.188	26.5	−7.86	9.53	3.12
				Orthorhombic phase (208 K)					
O180{1$\bar{1}$0}†	2.66	31.0	8.20	1.70	0.331	26.5	−9.71	−2.75	4.36
O180{001}	0.70	8.9	8.95	1.64	0.331	2.0	−11.07	−2.13	4.36
O90	0.72	4.3	4.26	1.50	0.234	2.0	−11.62	−0.08	12.97
O60	3.62	5.3	1.09	1.08	0.166	26.1	−7.64	12.14	4.36
O120†	1.70	13.7	5.82	1.47	0.287	10.2	−10.82	0.50	4.92
				Rhombohedral phase (118 K)					
R180{1$\bar{1}$0}†	2.13	36.0	11.81	1.83	0.381	18.3	−9.53	−3.64	3.17
R180{$\bar{2}$11}†	2.13	36.0	11.81	1.83	0.381	18.3	−9.53	−3.64	3.17
R109†	0.70	7.8	7.81	1.65	0.311	2.0	−10.84	−2.56	5.60
R71	0.74	3.7	3.52	1.58	0.220	2.0	−10.31	−2.42	17.94

$=0.331$ C m^{-2}, $e_a=\frac{Q_{11}+Q_{12}}{2}P_0^2=3.58\times10^{-3}$, $e_c=Q_{12}P_0^2=-4.96\times10^{-3}$, and $e_b=\frac{Q_{44}}{4}P_0^2=0.79\times10^{-3}$ (the orthorhombic phase, 208 K); $P_0=0.381$ C m^{-2}, $e_a=\frac{Q_{11}+2Q_{12}}{3}P_0^2=0.97\times10^{-3}$, and $e_b=\frac{Q_{44}}{4}P_0^2=0.70\times10^{-3}$ (the rhombohedral phase, 118 K). The base vectors for the O60 domain wall [see Eq. (3)] at 208 K are

$$\mathbf{r}_{O60}=(0.707,0,0.707),$$

$$\mathbf{s}_{O60}=(0.701,0.130,-0.701),$$

$$\mathbf{t}_{O60}=(-0.092,0.991,0.092). \quad (28)$$

Right four columns of the Table III contain corresponding numerical values of the domain-wall coefficients g, a_1, a_{11}, and a_{111} derived from GLD parameters and spontaneous order-parameter values using above derived analytical expressions, mostly given explicitly in Table II. The left part of the Table III contains the key domain-wall properties such as wall thickness 2ξ and energy density Σ.

Clearly, T90 and O60 domain walls are considerably broader then others. T90 wall in the tetragonal phase is predicted to be 3.59 nm at 298 K (as already calculated in Ref. 4) and *S*-type O60 domain wall in the orthorhombic phase is predicted to be 3.62 nm at 208 K. Since the wall thickness is greater than the lattice spacing, the pinning of the walls is weak[22] and they can be easily moved. Moreover, in case of O60 wall, the pinning is further suppressed due to "incommensurate" character of Miller indices of the wall normal.

As follows from Eq. (23), domain-wall thickness is determined by quantities g, U, and p_∞. By inspection of their values in the Table III, we see that the most important factor is the coefficient g. Indeed the domain walls R71, R109, O90, O180{001}, and T180 with $g=2\times10^{-11}$ kg m^5 s^{-2} C^{-2} are all very narrow (thickness below 1 nm), and the thickness of various walls monotonically increases with increasing value of g. Let us stress that coefficients a_1, a_{11}, a_{111}, and g depend on the direction of the domain-wall normal. For example, O180{1$\bar{1}$0} with $g=26.5\times10^{-11}$ kg m^5 s^{-2} C^{-2} is almost four times broader than O180{001} with $g=2\times10^{-11}$ kg m^5 s^{-2} C^{-2}.

In the absence of other constraints, the probability of appearance of domain-wall species should be determined by the surface energy density Σ. Therefore, in the orthorhombic phase, the thinner O180{001} wall is more likely to occur than the 0180{1$\bar{1}$0} one. Interestingly, the O180{001} wall has almost the same thickness as the O90 wall while in the tetragonal phase, it is the 90° wall which is much thicker than 180° wall (3.59 nm compared to 0.63 nm).

In general, the normal of the neutral 180° domain wall can take any direction perpendicular to the spontaneous polarization of the adjacent domains. Therefore, also Σ depends on the orientation of the wall normal (in the *s*-*t* plane). We have checked in the orthorhombic phase that the O180{001} and 0180{1$\bar{1}$0} correspond to the extremes in the angular dependence of Σ, which is monotonous between them. This strong angular dependence is correlated with the anisotropy of the tensor G_{ijkl}. However, g is independent of the wall direction in the tetragonal and rhombohedral phase, and also

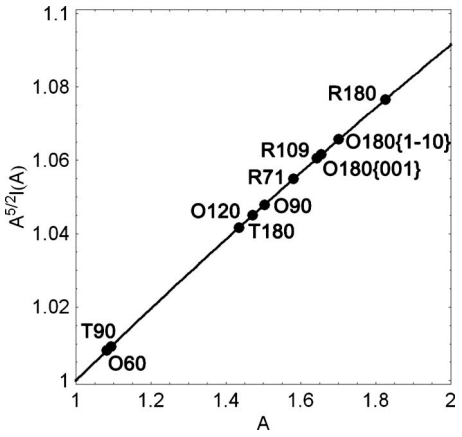

FIG. 4. Dependence of correction factor in the expression for domain-wall energy density [Eq. (25)] as a function of the shape coefficient A. Full points indicate values of A for particular domain walls considered in Table III.

the variation in coefficients a_1, a_{11}, and a_{111} is insignificantly small so that the effective directional dependence of 180° domain-wall properties in these phases is negligible.

The values of the shape factor A (see Table III) determines the deviation of the $P_r(s)$ polarization profile of the domain walls from the simple tanh form. For all studied cases the values of A range between 1 and 2, where the correction factor $A^{5/2}I(A)$ appearing in the Eq. (25) is almost linear function of A, as it can be seen in Fig. 4. It means that the shape deviations are much smaller than those shown by broken line in Fig. 3. Unfortunately, in the case of broad walls T90 and O60, which are good candidates for study of the structure of the wall central part, A is almost one.

Equation (14) can be also used to evaluate local strain variation in the wall. In Fig. 5, the profiles of strain-tensor components for T90 domain wall are shown for illustration. Obviously, e_{33}, e_{23}, and e_{13} strain components are strictly constant and equal to their boundary values as it follows from mechanical compatibility conditions. The e_{11} and e_{22} components and polarization P_r vary between their spontaneous values. Let us stress that the "reentrant" shear component e_{12} (it has the same value in both adjacent domains) approaches the nonzero value of about 5×10^{-4} in the middle of the domain wall.

The temperature dependence of the thickness and surface energy density of the 12 studied domain-wall species is plotted in Figs. 6(a) and 6(b), respectively. Although some properties do vary considerably, e.g., thickness of T90 wall in the vicinity of the paraelectric-ferroelectric phase transition, the sequence of the thickness values as well as the surface energy-density values of different domain-wall types remain conserved within each phase.

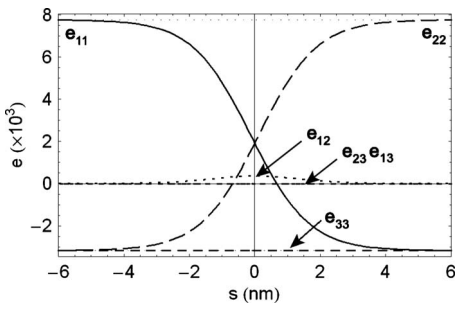

FIG. 5. Course of strain components along the domain-wall normal coordinate s for the T90 domain wall. Indices refer to cubic axes of the parent phase.

The temperature dependence of domain-wall thickness follows the trend given by Eq. (23). It increases with increasing temperature due to the dependence on p_∞ [see dependence of U on p_∞ in Eq. (24)], which decreases at the same time. Such behavior is well known also from the experimental observations.[3,23,24]

VI. CURVED POLARIZATION PATH SOLUTIONS

So far we have investigated domain walls within the SPP approximation, i.e., components P_s and P_t, which are the same in both domain states, were kept constant inside the whole wall. This is quite usual assumption made for a ferroelectric domain wall. Nevertheless, the full variational problem, where all three components of **P** could vary along **s** coordinate, lead in general to a lower-energy solution corresponding to a curved polarization path (CPP) in the three-dimensional primary order-parameter space. Appearance of the nonzero reentrant components within a ferroelectric domain wall was considered, e.g., in works of Refs. 3, 4, 25, and 26. For 180° walls, the polarization profile associated with SPP is sometimes denoted as the Ising-type wall. In contrast, the CPP solutions with nonzero P_s, P_t are often considered as Néel and Bloch-type,[26] even though, in contrast with magnetism, the modulus of **P** is far from being conserved along the wall normal **s**.

We have previously considered nonconstant P_s component of polarization in the 90° wall with explicit treatment of electrostatic interaction and realized that the deviations from SPP approximation are quite negligible.[4] In general, nonconstant P_s would lead to nonvanishing $\nabla\cdot\mathbf{P}$ and finite local charge density, which in a perfect dielectric causes a severe energy penalty. The same situation is expected for all domain-wall species. However, there is no such penalty for nonconstant P_t solutions. It was previously argued[3] that the Bloch-type (with a considerable magnitude of P_t at the domain-wall center) solutions could occur in orthorhombic $BaTiO_3$. Therefore, it is interesting to systematically check for existence of such solutions using our model.

In order to study such Bloch-type solutions, we have calculated Euler-Lagrange potential in the order-parameter plane $P_s=P_s(\pm\infty)$ by integrating Euler-Lagrange equations [Eqs. (13) and (14)] for all domain wall species from Table III similarly as, e.g., in the Refs. 1 and 3. Resulting two-dimensional Euler-Lagrange potential surfaces (ELPSs) are displayed in Fig. 7. In each ELPS, the bold lines indicate numerically obtained domain-wall solution with the lowest energy. The spatial step was chosen as 0.1 nm, P_r and P_t were fixed to boundary conditions in sufficient distance from domain wall (6 nm) and initial conditions for P_t were chosen so that the polarization path bypasses the energy maximum of the ELPS, and the system was relaxed to the equilibrium.

Among the 12 treated wall species, there are six cases where only the SPP solutions with P_t=const exist:

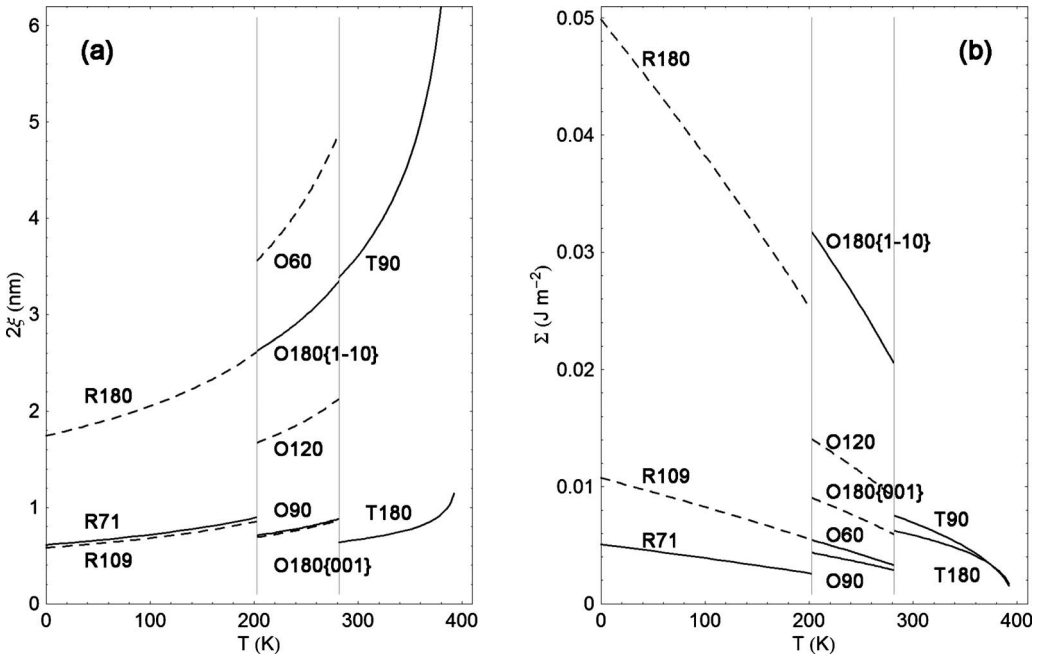

FIG. 6. Temperature dependence of the thickness (a) and energy density (b) for various mechanically compatible and neutral domain walls of $BaTiO_3$ estimated within SPP approximation. The SPP values for domain walls for which relaxing of the P_t component results in a lower-energy CPP solution are shown by dashed lines. Thickness of O180{001}, O90 has a very close temperature dependence. The results for T180 as well as for R180 walls are not distinguished by specific orientations of the wall normal since for both cases the angular dependence of thickness and energy of SPP solutions on the domain-wall normal is negligible (see Table III). Vertical lines mark phase-transition temperatures.

T180{001}, T180{011}, T90, O180{1$\bar{1}$0}, O90, and R71. These solutions are clearly "Ising-type." In all these cases, the (P_r=0, P_t=0) point is the only saddle point of the ELPS. In the other six cases—O180{001}, O60, O120, R180{1$\bar{1}$0}, R180{$\bar{2}$11}, and R109—the ELPS has a maximum at the (P_r=0, P_t=0), and the lowest-energy solutions correspond to curved polarization paths. This suggests that the previously discussed SPP description may not necessarily be the proper approximation for these walls. Nevertheless, in the case of O60 and O120 walls, the deviations from the SPP model are marginal, and only the remaining four solutions exhibit strong Bloch-type behavior. Moreover, the energy differences between SPP and CPP solutions were found to be almost negligible, except for R180, where the CPP energy is by about 10% lower in the entire temperature range of stability of the rhombohedral phase. Therefore, it is quite possible that in the case of O180{001}, R180{1$\bar{1}$0}, R180{$\bar{2}$11}, and R109 walls both Bloch-type and Ising-type solutions may be realized.

The deviations from SPP in the case of the almost Ising-type O60 and O120 walls are associated with the fact that ELPS is not symmetric with respect to P_t=$P_t(\pm\infty)$ mirror plane. In these cases, not only the polarization path and wall energies but also domain-wall thicknesses of the SPP and CPP counterpart solutions are very similar. This is demonstrated in Fig. 8, which shows polarization profiles of both SPP and CPP solutions for the O60 wall.

Much more pronounced difference between domain-wall profiles of SPP and CPP solutions are found in case of O180{001}, R180{1$\bar{1}$0}, R180{$\bar{2}$11}, and R109 Bloch-type walls where the CPP trajectories bypass the (P_r=0, P_t=0) maximum near the additional minima, which originate from "intermediate" domain states either of the same phase or even of the different ferroelectric phases. In these cases, the inadequacy of SPP approximation is obvious. For example, the CPP of R180{$\bar{2}$11} wall seems to pass through a additional minimum corresponding to an "orthorhombic" polarization state (consult corresponding inset in the Fig. 2). As expected, the profile of such CPP solution deviates strongly from tanh shape and even definition of the wall thickness would be problematic (see Fig. 9).

VII. CONCLUSION

The work reports detailed study of mechanically compatible and electrically neutral domain walls in $BaTiO_3$. The investigation was done within the framework of the GLD model. Using the SPP approximation, it was possible to compare properties of various kinds of domain-wall species from the same perspective.

The phenomenological nature of the GLD model allowed to predict the temperature dependence of the domain-wall characteristics in the whole temperature range of ferroelectric phases. Its continuous nature gave us even the opportunity to deal conveniently with the noncrystallographic *S*-type domain wall, which has a general orientation with respect to the crystal lattice, and which is therefore difficult to cope with in discrete models relying on periodic boundary conditions.

The *S* wall in the orthorhombic, as well as the 90° wall in tetragonal phase were both found to be about 4 nm thick and

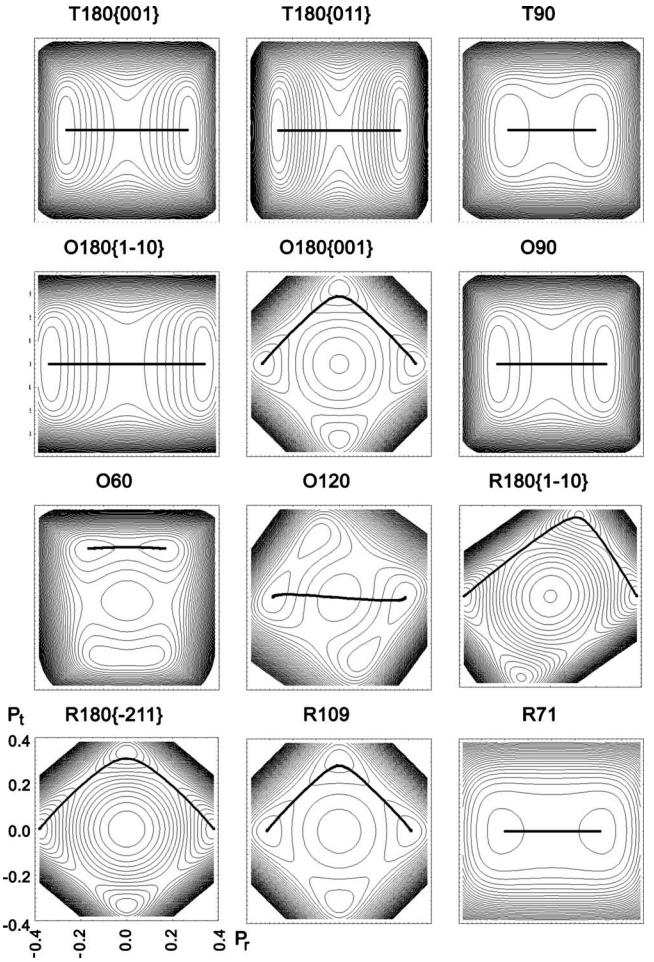

FIG. 7. Equipotential contours of the Euler-Lagrange potentials showing ELPS associated with the $P_s=P_s(\pm\infty)$ plane for a set of $BaTiO_3$ domain walls considered in Table III. Polarization scale given for the bottom left inset (in Cm^{-2}) is equally valid for all shown ELPSs. Energetically most favorable domain-wall solutions with trajectories restricted to the $P_s=P_s(\pm\infty)$ plane are indicated with bold lines. The solutions corresponding to a linear segment are denoted in the text as SPP walls, as opposed to the CPP solutions which have a curved order-parameter trajectory.

consequently are expected to be mobile, i.e., they could be easily driven by external fields, and they may thus significantly contribute to the dielectric or piezoelectric response of the material.

For several temperatures, we have numerically investigated domain walls allowing for more complicated CPP solutions with nonconstant P_t. We have identified solutions, which could be considered as analogues of Bloch walls known from magnetism. Interestingly, in contrast with Ref. 3, our model predicts the Ising-type profile of the O180$\{1\bar{1}0\}$ wall. At the same time, the Bloch-type structure of the O180{001} wall is predicted.

We believe that this kind of somewhat exotic walls actually represent important generic examples of ferroelectric domain species, which should be anticipated in all ferroelectrics with several equivalent domain states distinguished simultaneously by the orientation of the spontaneous polarization and strain. They should be certainly taken into account in investigations of domain-wall phenomena in ferroelectric perovskites. At the same time, the energy differences between the Bloch-type and Ising-type solutions are rather subtle here. Therefore, in spite of the fairly good agreement for 180° and 90° domain walls between *ab initio* calculations

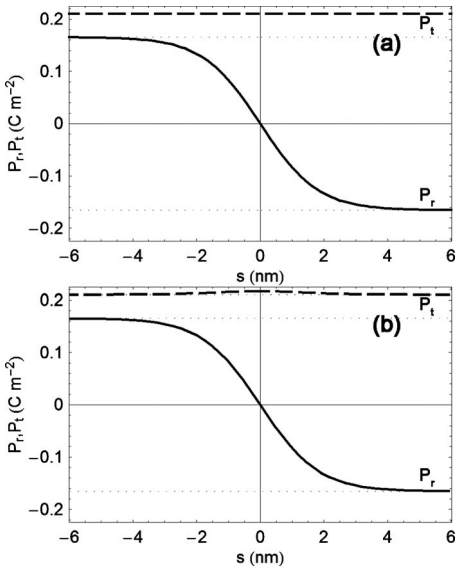

FIG. 8. Predicted profiles of polarization components for O60 domain wall in $BaTiO_3$ at $T=208$ K. Full line stands for the P_r component of polarization vector and broken line for the P_t one. Analytically obtained (a) SPP solution practically does not differ from the numerically obtained (b) CPP solution with an unconstrained P_t component in this case.

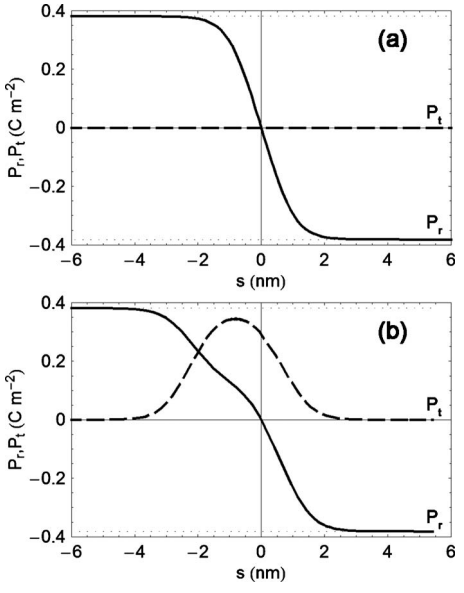

FIG. 9. Profiles of polarization components in R180$\{1\bar{1}0\}$ domain wall showing (a) the SPP stationary trajectory as well as the (b) lower-energy Bloch-type solution, both for the model parameters corresponding to $T=118$ K. Full line stands for the P_r component of polarization vector and broken line for the P_t one. The bottom panel demonstrates that Bloch solution may considerable modify the domain-wall profile.

and predictions of this model in the tetragonal phase,[4] the preference for the calculated Bloch-type trajectories may not necessarily reproduced for the domain walls encountered in real $BaTiO_3$ crystal since there is obviously a considerable uncertainty in the adopted material-specific GLD parameters. In addition, predictions for the domain walls with very small thickness must be considered with a particular caution since the description of the sharp domain-wall profiles obviously touches the limits of the applicability of the continuous model.

In conclusion, progress in controlling of domains and domain walls is expected to influence significantly the electromechanical properties of the current ferroelectric perovskite materials and for that reason, a detailed knowledge of the domain-wall properties is desirable.[16,27,28] We have derived a number of qualitative and quantitative predictions for mechanically compatible neutral domain walls of tetragonal, orthorhombic, and rhombohedral $BaTiO_3$ on the basis of the previously proposed material-specific GLD model. We believe that the insight into the domain-wall properties mediated by the provided analytical and numerical analysis could be helpful for understanding of domain-wall phenomena in $BaTiO_3$ as well as in some other intensively investigated members of the ferroelectric perovskite family with same sort of macroscopic ferroelectric phases, for example, in $KNbO_3$, $BiFeO_3$, $PbTiO_3$, or even PZT and perovskite relaxor-related materials.

ACKNOWLEDGMENTS

The authors are grateful to V. Janovec for helpful comments and critical reading of the manuscript. This work has been supported by the Czech Science Foundation (Projects No. P204/10/0616 and No. 202/09/0430) and by the Academy of Sciences of the Czech Republic (Project No. AVOZ 10100520).

[1] W. Cao and L. E. Cross, Phys. Rev. B **44**, 5 (1991).
[2] Y. Ishibashi and E. Salje, J. Phys. Soc. Jpn. **71**, 2800 (2002).
[3] X. R. Huang, S. S. Jiang, X. B. Hu, and W. J. Liu, J. Phys.: Condens. Matter **9**, 4467 (1997).
[4] J. Hlinka and P. Marton, Phys. Rev. B **74**, 104104 (2006).
[5] J. Erhart, W. Cao, and J. Fousek, Ferroelectrics **252**, 137 (2001).
[6] S. Nambu and D. A. Sagala, Phys. Rev. B **50**, 5838 (1994).
[7] H. L. Hu and L. Q. Chen, J. Am. Ceram. Soc. **81**, 492 (1998).
[8] R. Ahluwalia, T. Lookman, A. Saxena, and W. Cao, Appl. Phys. Lett. **84**, 3450 (2004).
[9] P. Marton and J. Hlinka, Phase Transitions **79**, 467 (2006).
[10] J. Fousek and V. Janovec, J. Appl. Phys. **40**, 135 (1969).
[11] V. Janovec and J. Privratska, *International Tables for Crystallography* (Kluwer Academic, Dordrecht, 2003), Vol. D, Chap. 3.4.
[12] J. Fousek, Czech. J. Phys., Sect. B **21**, 955 (1971).
[13] Similar calculations can be performed with a potential expanded to the eighth order in polarization. Nevertheless, in our previous calculations of domain wall profiles of tetragonal $BaTiO_3$, we have not observed any significant difference between the results obtained within the sixth-order and the eighth-order models. Also, for most of the perovskite ferroelectrics, the numerical coefficients of eighth-order expansion model are not known with a sufficient precision. Therefore, the calculations presented here are limited to the sixth-order expansion, which also allows to express more results in simple analytical form.
[14] A. J. Bell, J. Appl. Phys. **89**, 3907 (2001).
[15] In the final phase of preparation of this paper, it turned out that the value of q_{44} should be multiplied by a factor of 2 (Ref. 16). Considering the general character of this paper, we have left the original value of q_{44}, which is being used in some previous works referred to here. The changes in results are minor ones and they can be traced using provided analytical expressions.
[16] J. Hlinka, P. Ondrejkovic, and P. Marton, Nanotechnology **20**, 105709 (2009).
[17] V. A. Zhirnov, Zh. Eksp. Teor. Fiz. **35**, 1175 (1958) [Sov. Phys. JETP **8**, 822 (1959)].
[18] O. Hudak, arXiv:cond-mat/0504701 (unpublished).
[19] Y. Ishibashi and V. Dvorak, J. Phys. Soc. Jpn. **41**, 1650 (1976).
[20] B. Houchmandzadeh, J. Lajzerowic, and E. Salje, J. Phys.: Condens. Matter **3**, 5163 (1991).
[21] J. Hlinka and P. Marton, Integr. Ferroelectr. **101**, 50 (2008).
[22] Y. Ishibashi, J. Phys. Soc. Jpn. **46**, 1254 (1979).
[23] M. Robert, I. Reaney, and P. Stadelmann, Physica A **229**, 47 (1996).
[24] S. R. Andrews and R. A. Cowley, J. Phys. C **19**, 615 (1986).
[25] B. Meyer and D. Vanderbilt, Phys. Rev. B **65**, 104111 (2002).
[26] D. Lee, R. K. Behera, P. Wu, H. Xu, Y. L. Li, S. B. Sinnott, S. R. Phillpot, L. Q. Chen, and V. Gopalan, Phys. Rev. B **80**, 060102(R) (2009).
[27] H. Cao, C. P. Devreugd, W. Ge, J. Li, D. Viehland, H. Luo, and X. Zhao, Appl. Phys. Lett. **94**, 032901 (2009).
[28] E. Burcsu, V. Ravichandran, and K. Bhattacharya, J. Mech. Phys. Solids **52**, 823 (2004).